Initiation mechanisms of fatigue cracks in carbon black filled natural rubber

Bertrand Huneau, Isaure Masquelier, Yann Marco, Vincent Le Saux, Simon Noizet, Clémentine Schiel, Pierre Charrier

Initiation mechanisms of fatigue cracks in carbon black filled natural rubber

B. Huneau
Ecole Centrale de Nantes, Institut de Recherche en Génie Civil et Mécanique (GeM), UMR CNRS 6183, Nantes, France

I. Masquelier, Y. Marco & V. Le Saux
ENSTA Bretagne, Laboratoire Brestois de Mécanique des Structures (LBMS), Brest, France

S. Noizet, C. Schiel & P. Charrier
CAE Durability Prediction Department, Trelleborg Vibracoustic Group, Carquefou, France

ABSTRACT: A thorough analysis of the initiation stage of fatigue cracks in carbon black filled natural rubber is conducted. This study is based on interrupted tests: fatigued samples are observed with scanning electron microscope and analyzed with energy dispersive spectrometry of x-rays, in order to characterize the morphology and the chemical composition of the microstructural defects leading to the initiation of fatigue cracks. This procedure allows to quantify the spatial distribution and the evolution of crack initiation sites for different strain levels. It also reveals that inclusions such as carbon black agglomerates or ZnO are generally responsible for the initiation. However, those two types of inclusions correspond to different crack initiation mechanisms and, most of the time, only the initiations on carbon black agglomerates are followed by crack propagation that leads to failure. The carbon black agglomerates appear to have a stronger cohesion than ZnO inclusions and a stronger adhesion to the matrix. Consequently, two kinds of initiation mechanisms are proposed considering the nature of the inclusions, their cohesion and their interface properties with the matrix.

1 INTRODUCTION

For filled Natural Rubber (NR), fatigue crack initiation generally occurs at the surface or subsurface and in most of the cases, initiation sites are inclusions: filler agglomerates (silica or carbon black) or oxides, such as zinc oxide (Saintier et al. 2006, Bennani 2006, Le Gorju Jago 2007, Le Cam et al. 2013). The size of these inclusions ranges from a few microns to a few hundreds of microns. This was confirmed in a previous study in which we followed the damage of a sample all along its fatigue life (Huneau et al. 2013). However, the precise damage mechanisms leading to the initiation had not been well understood. A recent study has allowed us to clarify this point (Masquelier 2014).

The damage induced by fatigue loading in rubber can be investigated by different experimental techniques. Among them, Scanning Electron Microscope (SEM) is a powerful tool to observe either fatigue fracture surfaces (Bhowmick et al. 1980, Le Cam et al. 2013) or interrupted fatigued samples to acquire more precise information about the mechanisms of crack initiation and crack propagation (Le Cam et al. 2004, Saintier et al. 2006, Hainsworth 2007, Beurrot et al. 2010, Flamm et al. 2011). Nevertheless, these studies rarely focus only on crack initiation, probably because this phenomenon is not easily predictable, in terms of location (where are the crack initiated?) and time (after how many cycles?).

The first objective of this study is to obtain some statistical information about fatigue crack initiation sites: location, distribution, nature and evolution, by SEM observations of the whole damaged surface of the samples at different moments in the fatigue life.

The second objective is to describe the crack initiation mechanisms for the two main types of inclusions responsible for the initiation.

The experimental procedure will be detailed in Section 2. Then, the results concerning the description of fatigue crack initiation and the related mechanisms will be presented and discussed in Section 3.

2 EXPERIMENTAL PROCEDURE

2.1 *Material and samples*

The compounds are Natural Rubbers (NR) filled with Carbon Black (CB) and vulcanized

with sulphur. The chemical composition is given in Table 1.

Most of the results presented here are obtained on a NR filled with CB N550 type, but in Section 3.4.1 we also use results obtained with other CB types: N220, N326, N375, N772. For the latter type, CB amount is raised to 50 phr in order to have stiffness comparable to the ones of the other materials.

In the following, the material's reference includes CB content and CB type. For example, the main studied compound is referred to as NR43-N550.

2.2 *Fatigue tests*

Fatigue tests are performed on hourglass-shaped specimens (referred to as AE2 in the following) and shown in Figure 1a. The median zone of those specimens is 10 mm in diameter. Because of this particular geometry the strain field is very heterogeneous. The maximum strains are reached at the surface of the sample and are calculated by FEA. The fatigue results are plotted with the maximum principal strain in the median zone (slice 1, Fig. 1b). The lower strains in slices 2/2′ and 3/3′ will be considered to investigate the influence of strain level on the number of initiation sites (Fig. 1b).

All the fatigue tests were conducted at TrelleborgVibracoustic on a specific device. They are monitored with prescribed displacement and for a minimum displacement equal to zero. The frequency of the tests varies from 1 Hz to 5 Hz. By using 25 specimens, a Wöhler curve, shown in Figure 2, is plotted with the maximum principal strain as a function of the number of cycles corresponding to the end of life of the specimens. This number is called Ni and is detected by a loss of the specimen stiffness: see Ostoja-Koczynski et al. (2003) for the details. This Wöhler curve is used as a reference to define the strain level and the number of cycles for each sequence of the interrupted fatigue tests.

In our previous study (Huneau et al. 2013), we investigated the damage evolution along the fatigue life by following the same sample. Here the following protocol is used for the interrupted fatigue tests: each sample is subjected to one of the three strain levels (60%, 100% and 200%) and to one of the three percentages of fatigue life (20% Ni, 40% Ni and 60% Ni). Consequently 9 samples were observed. This particular protocol is chosen to avoid the cumulative damage that can be caused by the electron beam of the SEM, when one follows the same sample, and also to have statistical information.

Table 1. Composition of the NR compounds.

	Amount
Ingredient	Parts per hundred rubber (phr)
NR gum	100
Carbon Black (CB)	43
Sulphur	1.8
CBS	2.5
Zinc oxide	5.0

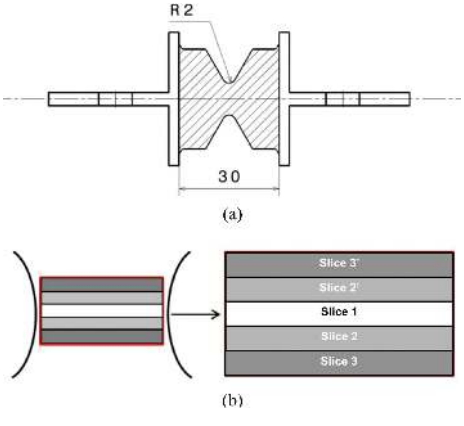

Figure 1. (a) Geometry of the AE2 sample, (b) observed zone and definition of the different slices.

2.3 *Scanning Electron Microscope (SEM)*

The SEM investigations are performed with a JEOL 6060-LA. The acceleration voltage is 20 kV and the images are taken by using the secondary electrons signal. The chemical composition of inclusions is determined thanks to an Energy Dispersive Spectrometer (EDS) of X-rays.

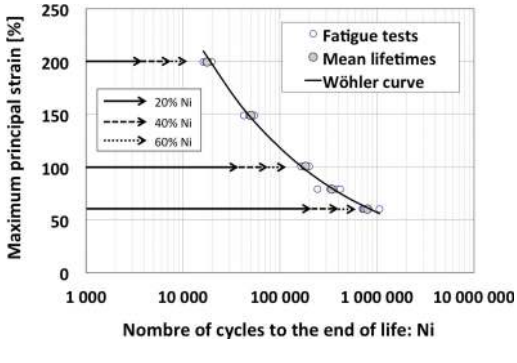

Figure 2. Wöhler curve obtained on NR43-N550 with the three strain levels investigated and the three percentages of fatigue life (% Ni).

Observations are performed on fatigued samples stretched of 3 mm. The observed zone, which is 3.75 mm in height and 6.9 mm in width, is analyzed throughout five slices (Fig. 1b). In order to observe the whole circumference of the samples, this operation is repeated 4 times, after successive rotations of 90°. For one sample, 140 SEM images are taken (7 per slices × 5 slices × 4 sides).

3 RESULTS AND DISCUSSION

3.1 *Damage mechanisms in fatigue*

For the considered experimental conditions and elastomers, the fatigue loading always induces a multi-cracking phenomenon. The numerous cracks observed are initiated either at the parting line or out of the parting line (Fig. 3). This was first observed on fracture surfaces and then confirmed by the interrupted fatigue tests. These interrupted tests also reveal that the initiation of cracks starts very early in the fatigue life and that the propagation stage is relatively slow. The multi-initiation and the low fatigue crack growth rates can explain the low dispersion obtained in fatigue lives (Fig. 2).

3.2 *Influence of the number of cycles and of the maximum principal strain*

The density of surface cracks (longer than 5 µm) is plotted in Figure 4 for the three percentages of the fatigue life Ni (20%, 40%, 60%) and for the different local strains obtained for the three fatigue levels: 60%, 100%, 200% maximum principal strain. These maximum values are related to the observations made in slice 1 (Fig. 1). Additionally, the results obtained in slices 2/2′ and in slices 3/3′ are plotted with their corresponding strain calculated by FEA.

Figure 4 clearly illustrates that the density of cracks increases with the percentage of fatigue life, which means that new crack initiation sites are activated all along the fatigue life. As expected, the density of cracks also increases with the strain level.

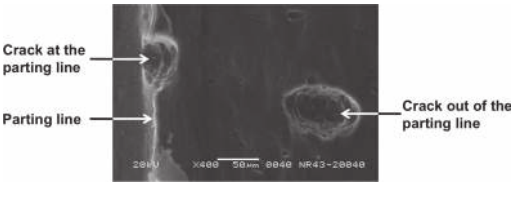

Figure 3. SEM picture of the typical locations of crack initiation sites: at the parting line or out of the parting line.

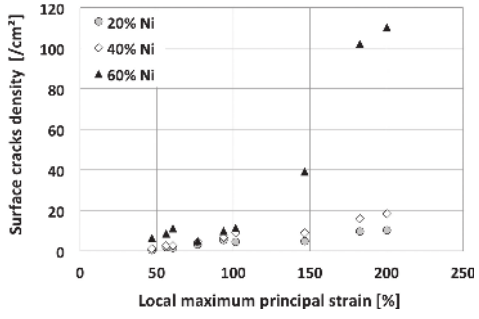

Figure 4. Density of surface cracks with respect to the maximum principal local strain for the three percentages of fatigue life (% Ni).

3.3 *Nature of the inclusions and criticality*

As mentioned in Section 3.1, the cracks are initiated either at the parting line, which can be considered as a geometrical defect acting as a stress concentrator, or around inclusions. In the following, the attention is focused only on cracks that are initiated on inclusions.

The main inclusions that appear to be responsible for fatigue crack initiation are: agglomerates of CB and inclusions of zinc oxide (ZnO) which are both ingredients of the recipe, and also other oxides such as talc, oxides containing aluminium and silicon (probably kaolinite, referred to as AlSiO in the following), or calcium/silicon oxides (CaO, SiO_2). Those oxides can be introduced into the materials by: the NR gum that contains some impurities, the covering powder of the sulphur and CBS pellets or the process (minor pollution due to a previous mixing/injection for example).

To investigate the relationship between the chemical nature of the inclusions and their criticality for crack initiation, the size of the cracks are compared to the size of the inclusions for various kinds of inclusions and for the three strain levels (Fig. 5).

On the three graphs of Figure 5, the line (having a slope of 1) corresponds to sites that do not give rise to the propagation of a crack, as the crack length is equal to the size of the inclusion. In that case, the sites are considered 'activated': there is some visible damage around the inclusion (cavity), but the size of the cavity is not bigger than the size of the inclusion (see Section 3.4 for more details). Critical cracks are therefore those whose length is much higher than the size of the inclusion responsible for its initiation.

From Figure 5, it can be seen that for the three strain levels CB agglomerates are the inclusions leading to the longer cracks; those that are initiated by the other types of inclusions propagate

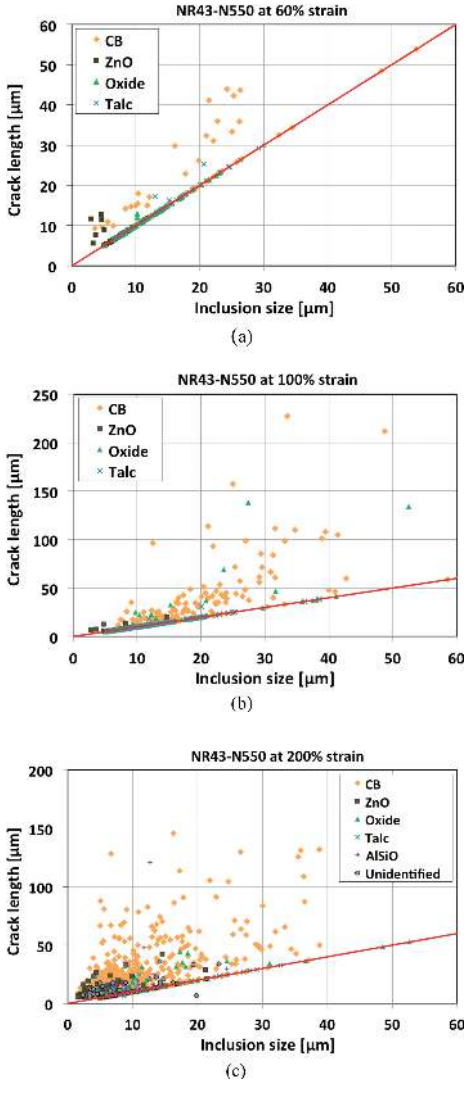

Figure 5. Size of the cracks vs. size of the inclusions for the three strain levels: (a) 60%, (b) 100%, (c) 200%.

only a little or not at all. However, it can be noted that a relatively high number of activated sites is due to ZnO inclusions (up to 40%), even if they appear to be less deleterious. This could be due to their relatively small size with most of them being smaller than 10 µm. The initiation mechanisms of fatigue cracks due to those two types of inclusions are more deeply investigated in the next Section.

3.4 *Fatigue crack initiation mechanisms*

In this last Section, the initiation mechanism associated with either CB agglomerates or ZnO inclusions are described. We will also try to find out what drives the initiation: a critical mechanical quantity and/or energy accumulation?

3.4.1 *For carbon black agglomerates*

From the analysis of the SEM images, the fatigue crack initiation mechanism around CB agglomerates can be divided into three stages represented in Figure 6:

- Stage 1: debonding at the pole;
- Stage 2: opening on the sides;
- Stage 3: growth at the surface and in the volume, which can be also considered as the early stages of crack propagation.

Stages 1 and 2 are associated with the initiation and are driven by the inclusion and its interface with the matrix, while the matrix controls Stage 3, with no influence of the inclusion. Cracks in Stage 3 show some ligaments at the crack tip, which is in agreement with the literature (Beurrot et al. 2010). Figure 7 shows schematically the initiation mechanism from the initial situation, or Stage 0, to the propagation (Stage 3).

CB agglomerates observed in the present study seem to have high internal cohesion (no broken agglomerates were observed) and good interface properties, i.e. a good adhesion to the matrix. The initiation mechanism occurs here by debonding, showing that the internal cohesion of the agglomerates is stronger than the filler/matrix interface. We remark also that all CB agglomerates exhibit a spherical shape. It suggests that, during the mixing, the CB pellets could be first broken and then

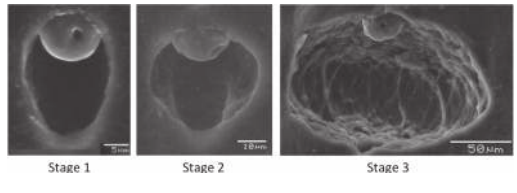

Figure 6. The three stages of fatigue crack initiation around a CB agglomerate: debonding at one pole (Stage 1), opening on the sides (Stage 2), growth at the surface and in the volume (Stage 3).

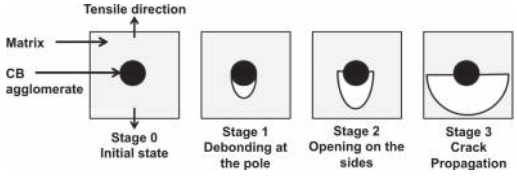

Figure 7. Schematic representation of fatigue crack initiation mechanism around a CB agglomerate.

eroded, producing the spherical shape. Those two mechanisms are classically involved in the dispersion of CB (Collin & Peuvrel-Disdier 2005). In order to see the internal structure and composition of such agglomerates, one of them has been collected and fractured between two small glass slides used for optical microscopy. Besides the fact that the fracture is very brittle (suggesting no or little occluded rubber), it appears to be homogeneous in terms of composition and appearance (data not shown here). Consequently, CB agglomerates do not seem to be covered by a layer of rubber. This would confirm a debonding mechanism rather than cavitation in the matrix.

As shown in Figure 8, at 100% strain the percentage of flaws in Stage 1 decreases during the fatigue life while the percentages of flaws in Stages 2 and 3 increase. These evolutions, also observed at 200% strain (data not shown here), tend to validate the proposed mechanism, in so far as it is progressive, and confirms that the CB agglomerates are responsible for the critical cracks (Stage 3).

To determine whether initiation is driven by an accumulation of energy and/or requires a critical mechanical quantity, the minimal size of CB agglomerates generating initiation is followed for each Stage and reported in Table 2 for the different strain levels and fatigue life percentages.

In Table 2, it can be seen on one hand that, for Stages 2 and 3 and for a given strain level, the minimum size of the flaws decreases when the percentage of fatigue life increases. This suggests that the transition from Stage 1 to 2 and from Stage 2 to 3 requires an accumulation of energy: the inclusions involved in the different damage stages are progressively smaller along the fatigue life. The associated cracks need a certain number of cycles, i.e. a certain amount of energy (cumulative damage?), to be created. On the other hand, for Stages 2 and 3, for the same percentage of fatigue life, the minimum size decreases when the strain level increases,

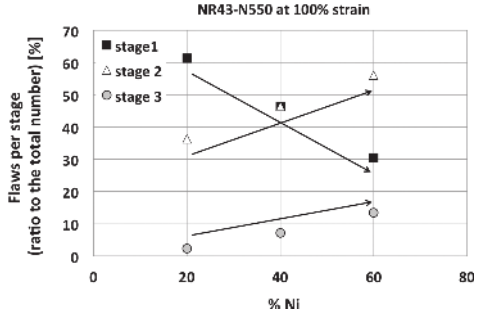

Figure 8. Evolution of the three stages for flaws associated with CB agglomerates in NR43-N550 at 100% strain with respect to the percentage of fatigue life (%Ni).

Table 2. Minimum size (s_{min}) of the CB agglomerates, for each stage (S1, S2, S3) vs. the strain and the % of fatigue life (%Ni).

Strain (%)	% Ni	s_{min} S1 (µm)	s_{min} S2 (µm)	s_{min} S3 (µm)
60	20	5.2	16.5	None
	40	6.2	10.2	None
	60	3.0	3.6	None
100	20	5.1	7.4	41
	40	4.8	3.5	12.4
	60	5.2	2.7	14.4
200	20	5.0	3.3	17.3
	40	5.1	3.2	3.4
	60	2.8	1.5	2.0

suggesting that a critical mechanical value has to be reached to create cracks and to start to propagate them.

Consequently, it seems that the different stages of the initiation mechanism involving CB agglomerates require both energy accumulation and critical mechanical value.

Finally, the question of the influence of the average size of CB agglomerates (on which cracks are initiated) on the fatigue end of life arises. To consider this question, an additional study has been conducted by using NR filled with five different CB types. Figure 9 reports the fatigue end of life at 100% strain with respect to the average size of the CB agglomerates for these five materials. As expected, it proves that bigger CB agglomerates shorten the fatigue life. Even if this result is logical and known for a long time for other materials (see for example (Murakami et al. 1989) who studied this effect on steels), it is here clearly demonstrated in the case of CB filled NR on the basis of a large number of observations.

3.4.2 *For zinc oxide inclusions*

The ZnO inclusions are responsible for many initiations of cracks that in most cases do not propagate. Indeed, considering the definition of the three stages previously established, we find very few flaws in Stage 3, and a majority in Stage 1, regardless of the strain level. The analysis of the SEM images shows that there are two mechanisms for Stage 1:

– fracture of the inclusion, in the case where the internal cohesive energy of the inclusion is smaller than the bonding to the matrix (Fig. 10a);
– debonding at one pole or at both poles, in the opposite situation (Fig. 10b, c).

ZnO are inclusions with low internal cohesion and low adhesion to the matrix. This explains that

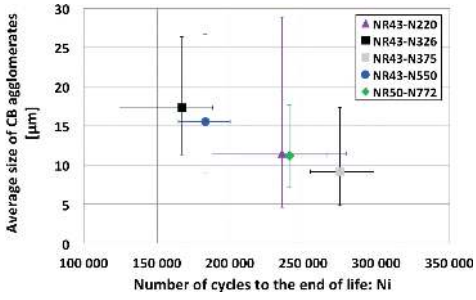

Figure 9. Size of the CB agglomerates on which cracks are initiated with respect to the fatigue end of life at 100% strain, for different types of CB.

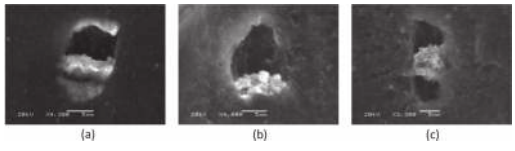

Figure 10. The different kinds of fatigue crack initiation mechanisms around ZnO (Stage 1): (a) fracture of the ZnO, (b) debonding at one pole, (c) debonding at both poles.

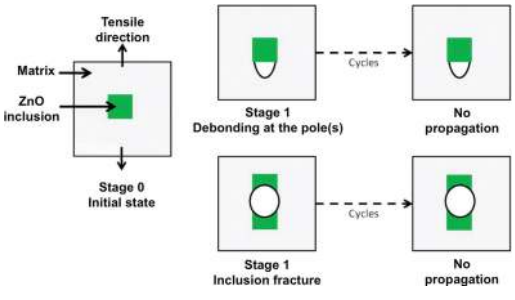

Figure 11. Schematic representation of the two different ways for crack initiation (Stage 1) around ZnO.

initiation can be easily activated (Stage 1) but rarely followed by the growth of long cracks (Stage 3). Figure 11 shows schematically the initiation mechanisms for Stage 1 around a ZnO inclusion.

If one considers the average size of ZnO inclusions activated (Stage 1) with respect to the percentage of fatigue life, it depends neither on the number of cycles nor on the strain level. This suggests that initiation does not require energy accumulation in this case. If there is a critical mechanical value necessary for initiation, it is reached from 60% strain, as the size does not change with the strain level.

The size of ZnO inclusions may explain why, in some particular cases, they lead to crack propagation. The size of ZnO associated with the rare Stage 3 cracks is between 14.6 µm and 28.7 µm, which is above the average size of ZnO (7 µm) and close or even higher than the average size of CB agglomerates (varying from 9 µm and 17 µm). This suggests that the size of the inclusion is crucial for the propagation. However, it is surprising that some "big" inclusions of ZnO (greater than 20 µm) do not generate crack propagation. The shape of the inclusion, which contributes to the properties of the interface, also probably plays an important role.

4 CONCLUSION

In the case of CB filled NR, fatigue damage is due to multi-cracking at the surface of the samples initiated on geometric accidents (parting line) and on inclusions.

The number of cracks increases with the number of cycles and with the strain level.

Analysis of the initiation sites around inclusions shows that they are of different types, including two types of inclusions playing a predominant role: CB agglomerates and ZnO inclusions.

CB agglomerates by their chemical composition and their spherical shape have a high cohesive energy and a good adhesion to the matrix. Crack initiation mechanism involves three steps: debonding at the interface (meaning that the internal cohesion is stronger than the bonding between inclusion and matrix), opening on the sides and then cracking at the surface and in the volume. Finally, at 100% strain for NR filled with different CB types, fatigue life appears to be related to the average size of the CB agglomerates: the end of life increases when the average agglomerate size decreases.

The internal cohesion of ZnO inclusions as well as their interface properties with the matrix are weak. Consequently, initiation occurs by debonding or fracture of the inclusion and does not seem to be progressive. In most cases, the created crack does not propagate.

ACKNOWLEDGEMENT

The authors would like to thank the ANR for its financial support (ANR–2010–RMNP-010-01) and all the partners of the PROFEM project: TrelleborgVibracoustic, LMBS, GeM, UBS and LRCCP.

REFERENCES

Bennani, A. 2006. *Elaboration, comportement et durée de vie en fatigue du caoutchouc naturel renforcé de silice*. PhD thesis, École Nationale Supérieure des Mines de Paris.

Beurrot, S., B. Huneau & E. Verron 2010. In situ SEM study of fatigue crack growth mechanism in carbon black-filled natural rubber. *Journal of Applied Polymer Science,* 117, 1260–1269.

Bhowmick, A.K., G.B. Nando, S. Basu & S.K. De 1980. Scanning electron microscopy studies of fractures natural rubber surfaces. *Rubber Chemistry and Technology,* 53, 327–334.

Collin, V. & E. Peuvrel-Disdier 2005. Dispersion mechanisms of carbon black in an elastomer matrix. *Elastomery,* 9, 9–15.

Flamm, M., J. Spreckels, T. Steinweger & U. Weltin 2011. Effects of very high loads on fatigue life of NR elastomer materials. *International Journal of Fatigue,* 33, 1189–1198.

Hainsworth, S.V. 2007. An environmental scanning electron microscopy investigation of fatigue crack initiation and propagation in elastomers. *Polymer Testing,* 26, 60–70.

Huneau, B., I. Masquelier, Y. Marco, O. Brzokewicz & P. Charrier 2013. Fatigue damage in carbon black filled natural rubber investigated by X-ray microtomography and scanning electron microscopy. *In*: N. Gil-Negrete & A. Alonso (eds), *Constitutive Models for Rubber VIII*, 2013 San Sebastian. CRC Press—Taylor & Francis, 393–398.

Le Cam, J.B., B. Huneau & E. Verron 2013. Fatigue damage in carbon black filled natural rubber under uni- and multiaxial loading conditions. *International Journal of Fatigue,* 52, 82–94.

Le Cam, J.B., B. Huneau, E. Verron & L. Gornet 2004. Mechanism of fatigue crack growth in carbon black filled natural rubber. *Macromolecules,* 37, 5011–5017.

Le Gorju Jago, K. 2007. Fatigue life of rubber components: 3D damage evolution from X-ray computed microtomography. *In:* A. Boukamel, L. Laiarinandrasana, S. Méo & E. Verron (eds), *Constitutive Models for Rubber V*, 2007 Paris. Taylor & Francis/Balkema, 173–177.

Masquelier, I. 2014. *Influence de la formulation sur les propriétés en fatigue d'élastomères industriels*. PhD thesis, Université Bretagne Occidentale.

Murakami, Y., S. Kodama & S. Konuma 1989. Quantitative evaluation of effects of non-metallic inclusions on fatigue strength of high strength steels. *International Journal of Fatigue,* 11, 291–298.

Ostoja-Kuczynski, E., P. Charrier, E. Verron, G. Marckmann, L. Gornet & G. Chagnon 2003. Crack initiation in filled natural rubber: experimental database and macroscopic observations. *In:* J. Busfield & A. Muhr (eds), *Constitutive Models for Rubber III*, 2003 London. Taylor & Francis, 41–47.

Saintier, N., G. Cailletaud & R. Piques 2006. Crack initiation and propagation under multiaxial fatigue in a natural rubber. *International Journal of Fatigue,* 28, 61–72.